Research Article

Lakshmanan Anitha, Loganathan Vadivukarasi, Rajendran Selvamani*, Rossana Dimitri, and Francesco Tornabene

# Nonlinear poro thermal vibration and parametric excitation in a magneto-elastic embedded nanobeam using homotopy perturbation technique

https://doi.org/10.1515/cls-2024-0013
received June 01, 2024; accepted September 09, 2024

**Abstract:** The primary focus of this study is to analyze the nonlinear vibration patterns and parametric excitation of embedded Euler–Bernoulli nanobeams subjected to thermo-magneto-mechanical loads. The Euler–Bernoulli nanobeam is developed with external parametric excitation. By utilizing nonlocal continuum theory and nonlinear von Karman beam theory, the governing equation of motion is derived. Subsequently, the homotopy perturbation technique is employed to determine the vibration frequencies. Finally, the modulation equation of Euler–Bernoulli nanobeams is derived for simply supported boundary conditions. The impacts of magnetic potential, temperature, damping coefficient, Winkler coefficient, and nonlocal parameters are tested numerically on nonlinear frequency–amplitude and parametric excitation–amplitude responses. Results demonstrate that physical variables significantly influence both nonlinear frequency behavior and parametric excitation.

**Keywords:** nonlinear vibration, parametric excitation, porosity, thermo-magneto-mechanical load, Euler–Bernoulli nanobeam, homotopy perturbation technique

## 1 Introduction

The captivating electromechanical properties of carbon nanostructures, such as carbon nanotubes and nanobeams, have drawn significant interest from researchers and scholars in the fields of advanced materials and engineering design. These nanostructures have found applications in various electromechanical devices, including light translucency [1,2], vibratory systems [3–5], gas atom diagnosis [6], storage units [7], and composite materials [8]. However, despite the recognized importance of small-scale effects on the characteristics and properties of nanostructures, classical plate theory is insufficient for assessing size effects in these structures [9]. To address this limitation, nonlocal elasticity theory, introduced by Eringen [10], has been widely adopted to examine size effects in nanostructures. The implementation of nonlocal elasticity theory has led to numerous theoretical investigations and significant advancements [11–17]. Much of the current research on micro/nanobeams focuses on their nonlinear properties. Nonlinear or high-amplitude vibration of beams – whether nano or micro – subjected to significant displacements occupies a crucial position in the engineering literature. For instance, Şimşek [18,19] explored the nonlinear vibration of nanobeams using nonlocal elasticity and strain gradient theories, highlighting the impact of small-scale effects on the nonlinear frequency response. Nazemnezhad and Hosseini-Hashemi [20] examined the nonlinear vibration behavior of functionally graded (FG) nanobeams under different boundary conditions, emphasizing the influence of the gradient index on nonlinear vibration characteristics. Additionally, Nourbakhsh *et al.* [21] employed the von Karman theory to analyze the effect of nonlinearity on the nonlinear frequency response of microbeams. Further contributions include Oskouie *et al.* [22], who presented the nonlinear frequency response of viscoelastic Euler–Bernoulli nanobeams, emphasizing the impact of viscoelastic properties on

* **Corresponding author: Rajendran Selvamani,** Department of Mathematics, Karunya Institute of Technology and Sciences, Coimabtore, 641114, Tamil Nadu, India, e-mail: selvamani@karunya.edu
**Lakshmanan Anitha:** Department of Mathematics, Nehru Memorial College, Puthanampatti, Trichy, Tamil Nadu, India
**Loganathan Vadivukarasi:** Department of Mathematics, Nandha Arts and Science College, Erode, Tamil Nadu, India
**Rossana Dimitri, Francesco Tornabene:** Department of Innovation Engineering, University of Salento, Lecce, Italy

nonlinear vibration characteristics. Ghadiri *et al.* [23] utilized the multiple time scales method to study the nonlinear forced vibration of nanobeams experiencing a moving concentrated load supported by a viscoelastic foundation. He [24] investigated a coupling method that utilizes homotopy perturbation techniques (HPTs) for analyzing nonlinear problems. Barati [25] delved into nonlocal-strain gradient-forced vibration analysis of metal foam nanoplates, examining both uniform and graded porosities. Additional studies have explored various aspects of nanostructures. For example, Kováčik *et al.* [26] discussed the Poisson's ratio of closed-cell aluminum foams, while Pourjabari *et al.* [27] explored the influence of porosity on free and forced vibration characteristics of graphene platelet reinforcement composite nanostructures. Chen *et al.* [28] contributed by discussing the free and forced vibrations of shear deformable FG porous beams, while Mirjavadi *et al.* [29] analyzed the nonlinear free and forced vibrations of graphene nanoplatelet-reinforced microbeams, considering geometrical imperfections. He [30] provided a new interpretation of the HPT. Meanwhile, Eltaher *et al.* [31] examined the coupling effects of nonlocal and surface energy on the vibration analysis of nanobeams. Reddy [32] discussed nonlocal theories related to the bending, buckling, and vibration of beams, and Aydogdu [33] investigated a comprehensive nonlocal beam theory to analyze these behaviors in nanobeams. Researchers have also recognized the importance of parametric excitation in electromechanical systems, particularly in energy harvesting systems [34–36], where a Duffing oscillator simulates the performance of energy harvesters. Parametric excitation has also been used to study nonlinear vibration and stability in various structures [37]. Darabi and Ganesan [37] and Wang [38] analyzed the effect of van der Waals interaction on the instability of double-walled nanobeams under parametric excitation. Similarly, Krylov *et al.* [39] explored pull-in instability in microdevices under parametric excitation using Mathieu and Hill's equations. Yan *et al.* [40] provided insights into the behavior of Timoshenko beams subjected to parametric and external excitations. Moreover, Eringen [41,42] examined the theory of nonlocal polar elastic continua and related differential equations. Further studies by Reddy [43,44] have contributed to continuum mechanics and nonlocal nonlinear formulations for beam and plate bending, while Emam [45,46] explored static and dynamic analysis of post-buckling in geometrically imperfect composite beams. Murmu *et al.* [47] investigated the influence of in-plane magnetic fields on transverse vibration of graphene sheets, and Kitipornchai *et al.* [48] modeled vibration characteristics of multilayered graphene sheets. Additionally, researchers like Nayfeh and Mook [49], Nazemnezhad and Hosseini-Hashemi [20], and Azrar *et al.* [50,51] have contributed to the understanding of nonlinear oscillations and dynamic responses in beams. Characteristics and behaviors of various nanobeam configurations under different environmental and boundary conditions were investigated in previous studies [52–57].

Hence, a literature review suggests that the impacts of nonlinear vibration and parametric excitation of magneto-thermo elastic embedded nanobeams have not been extensively investigated in existing studies. This research conducts a thorough examination of the nonlinear vibration behaviors and parametric excitation effects on embedded Euler–Bernoulli nanobeams under thermo-magneto-mechanical loads, along with external parametric excitation. To begin, a succinct model of the nanobeam is developed, followed by the application of an external axial force to induce parametric excitation. Subsequently, employing the nonlocal continuum theory and nonlinear von Karman beam theory, the governing nonlinear differential equation of motion is derived. The HPT is then employed to solve this equation. Finally, the modulation equation and the dynamic instability of the Euler–Bernoulli nanobeam are derived, leading to an examination of both trivial and nontrivial steady-state solutions. Results demonstrate that the magnetic potential, temperature, damping coefficient, Winkler coefficient, and nonlocal parameters have a significant impact on both nonlinear frequency behavior and parametric excitation.

## 2 Modeling of porous metal nanobeam

The metal's material traits are contingent upon the distribution of voids or pores. These voids can be distributed uniformly or in non-uniform patterns. In cases of non-uniform distribution, it can be further categorized as symmetric (non-uniform 1) or asymmetric (non-uniform 2). Subsequently, the forthcoming section will introduce the expressions for the material properties, specifically the elastic modulus ($E$) and mass density ($\rho$), pertaining to metal foam [25].

$$E = E_2(1 - e_0\Upsilon),\ \rho = \rho_2\sqrt{(1 - e_0\Upsilon)}\ \text{(Uniform)}, \quad (2.1)$$

where $\Upsilon = \frac{1}{e_0} - \frac{1}{e_0}\left(\frac{2}{\pi}\sqrt{1 - e_0} - \frac{2}{\pi} + 1\right)^2$.

The above equation defines $\Upsilon$ as a function of the coefficient $e_0$, which relates to the pore amount in the metal foam. This variable $\Upsilon$ is used in the expression for $E$ and $\rho$ for uniformly distributed voids in metal foam.

$$E(z) = E_2\left(1 - e_0\cos\left(\frac{\pi z}{h}\right)\right), \rho(z) = \rho_2\left(1 - e_m\cos\left(\frac{\pi z}{h}\right)\right)(\text{Non-uniform 1}), \tag{2.2}$$

$$E(z) = E_2\left(1 - e_0\cos\left(\frac{\pi z}{2h} + \frac{\pi}{4}\right)\right), \rho(z) = \rho_2\left(1 - e_m\cos\left(\frac{\pi z}{h} + \frac{\pi}{4}\right)\right)(\text{Non-uniform 2}), \tag{2.3}$$

where $z$ is the spatial coordinate and $h$ is the characteristic thickness. In the above definitions, the index 2 refers to a material property at its highest value. Also, there are two coefficients $e_0$ and $e_m$ elated to pore amount and mass distribution as

$$e_0 = 1 - \frac{E_2}{E_1} = 1 - \frac{G_2}{G_1}, e_m = 1 - \sqrt{1 - e_0}, \tag{2.4}$$

where $E_1$ and $G_1$ are the elastic modulus and shear modulus of the metal without voids. $E_2$ and $G_2$ are the highest values of the elastic modulus and shear modulus in the presence of voids.

# 3 Formulating the problem

Figure 1 illustrates the schematic of a porous nanobeam embedded in a visco-Pasternak foundation, subjected to an axial force along the $x$-axis with a height $h$ and length $L$. The axial force is represented as a function undergoing harmonic excitation with frequency ($\bar{\Omega}$). Moreover, the vertical displacement of the nanobeam is indicated by $w$ along the $z$-axis.

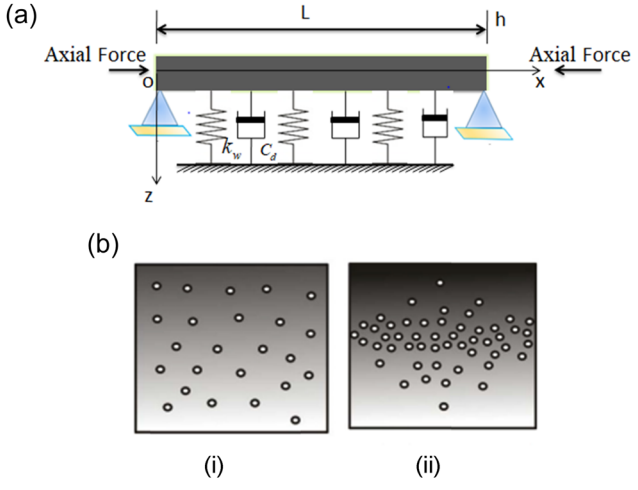


**Figure 1:** (a) Geometry of the beam. (b) Porosity distribution. (i) Uniform porosity. (ii) Non-uniform porosity.

## 3.1 Governing equations

In accordance with Eringen's nonlocal elasticity theory [9,10,41,42], the stress experienced at a reference point $X$ is postulated to be contingent upon the strain field throughout the body at each point $X'$. The nonlocal stress tensor $\sigma$ at point $X$ is formulated as follows:

$$\sigma = \int_V K(|X' - X|, \tau)\sigma'(X')\mathrm{d}X'. \tag{3.1}$$

Here $\sigma'$ denotes the classical stress tensor and $K(|X' - X|)$ represents the Kernel function, which signifies the nonlocal modulus. Eringen [10,42] illustrates that it is feasible to express the integral constitutive relation in an equivalent differential form as:

$$(1 - (e_0a)^2\nabla^2)\sigma = \sigma', \tag{3.2}$$

where $\nabla^2 = \frac{\partial^2}{\partial x^2} + \frac{\partial^2}{\partial y^2}$ represents the Laplacian operator, and $(e_0a)$ introduces the nonlocal parameter, where $e_0$ is a material-specific constant and $a$ is the internal characteristic length. The determination of the value of $e_0$ typically involves experimental methods or matching the dispersion relation of plane waves with those of atomic lattice dynamics. Subsequently, the nonlocal constitutive relation for the Euler–Bernoulli nanobeam can be expressed as:

$$\sigma_{xx} - (e_0a)^2\frac{\partial^2\sigma_{xx}}{\partial x^2} = E\varepsilon_{xx}, \tag{3.3}$$

where $\sigma_{xx}$ and $\varepsilon_{xx}$ denote the normal stress and strain, respectively, while $E$ represents Young's modulus. Following the Euler–Bernoulli beam model, the axial force and the resultant bending moment can be formulated as

$$\{N, M\} = \int_A \sigma_x(1, z)\mathrm{d}A, \tag{3.4}$$

where $z$ represents the transverse coordinate in the deflection direction, and $A$ denotes the area of the cross-section of the nanobeam. Utilizing the classical beam theory as outlined by Reddy [43,44], the displacements can be expressed as follows:

$$u_1(x, z, t) = u(x, t) - z\frac{\partial w}{\partial x}, u_2 = 0, \ u_3(x, z, t) = w(x, t). \tag{3.5}$$

In Eq. (3.5), $u$ and $w$ represent the axial and transverse displacements of the nanobeam along $x$ and $z$ directions, respectively. Now, considering the nonlinear von Karman strain, we can express it as:

$$\varepsilon = \varepsilon_0 + zk, \tag{3.6}$$

where $\varepsilon$ is the strain vector, and $\varepsilon_0$ and $k$ are the nonlinear strain vector and the change in the curvature vector, respectively, defined as follows:

$$\varepsilon_0 = \frac{\partial u_0}{\partial x} + \frac{1}{2}\left(\frac{\partial w}{\partial x}\right)^2,\ k = -\frac{\partial^2 w}{\partial x^2}. \tag{3.7}$$

In this context, $u_0$ represents the initial axial displacement in the strain expression, which captures the axial deformation before accounting for the additional effects due to transverse displacements and curvature. From Eqs. (3.3)–(3.7) the axial load and the bending moment are as follows:

$$(1 - (e_0a)^2\nabla^2)N = EA\varepsilon_0(1 - (e_0a)^2\nabla^2)M = EIk, \tag{3.8}$$

where $I = \int_A z^2 \mathrm{d}A$ represents the moment of inertia. Therefore, the equation of motion can be expressed as [45,46]:

$$\begin{aligned} EI\frac{\partial^4 w}{\partial x^4} - \frac{\partial}{\partial x}\left(N\frac{\partial w}{\partial x}\right) + (e_0a)^2\frac{\partial^3}{\partial x^3}\left(N\frac{\partial w}{\partial x}\right) \\ + \rho A\frac{\partial^2}{\partial t^2}\left[w - (e_0a)^2\frac{\partial^2 w}{\partial x^2}\right] = f - (e_0a)^2\frac{\partial^2 f}{\partial x^2}. \end{aligned} \tag{3.9}$$

The axial normal force $N$ can be determined as follows:

$$N = M_x + T_x + N_x + F\cos\Omega t - \left[\frac{EA}{2L}\int_0^L\left(\frac{\partial w}{\partial x}\right)^2 \mathrm{d}x. \right. \tag{3.10}$$

In Eq. (3.10), $M_x$, $T_x$, and $N_x$ represent a uniaxial magnetic field, thermal load caused by temperature change, and in-plane load caused by initial stress, respectively. Additionally, the term of $F\cos\Omega t$ is also the axial force capable of inducing parametric excitation, we can define the parameters of the axial normal force as follows:

$$M_x = \eta H_x^2\frac{\partial^2 w}{\partial x^2},\ \ T_x = \alpha EAT\ ,\ \ N_x = \xi\sigma_0. \tag{3.11}$$

Here $H_x$ and $\eta$ represent the in-plane uniaxial magnetic field and the magnetic field permeability, respectively. Specifically, $M_x$ explains the Lorentz force along the $x$-axis [47]. $T_x$, $\alpha$, $A$, and $T$ denote the coefficient of thermal expansion, the cross-sectional area, the difference between the temperature, and its initial reference temperature, respectively. Moreover, $\xi$ and $\sigma_0$ are the compression ratio and the initial stress, respectively. In this study, it is assumed that $\xi = 1$ and initial stress is along the $x$-axis direction. Additionally, in Eq. (3.9), $f$ is defined as follows:

$$f = K_{\mathrm{w}}w + c_{\mathrm{d}}\frac{\partial w}{\partial t}, \tag{3.12}$$

where $k_{\mathrm{w}}$ and $c_{\mathrm{d}}$ represent the linear coefficient of Winkler and damper modulus parameter, respectively. The Winkler-type foundation can be characterized based on the model from the study of Kitipornchai *et al.* [48]. Finally, to obtain the equation of motion, we substitute Eqs. (3.10)–(3.12) into Eq. (3.9) as follows:

$$\begin{aligned} -EI\frac{\partial^4 w}{\partial x^4} - \Bigg\{ & M_x + T_x + N_x + F\cos\Omega t \\ & - \left[\frac{\mathrm{EA}}{2L}\right]\int_0^L\left(\frac{\partial w}{\partial x}\right)^2 \mathrm{d}x\Bigg\}\frac{\partial^2 w}{\partial x^2} + c_d\frac{\partial w}{\partial t} \\ & + K_{\mathrm{w}}w\ \ T_x + N_x + F\cos\Omega t - \left[\frac{EA}{2L}\right]\int_0^L\left(\frac{\partial w}{\partial x}\right)^2 \mathrm{d}x\Bigg\} \\ & - (e_0a)^2K_{\mathrm{w}}\frac{\partial^2 w}{\partial x^2} - (e_0a)^2c_{\mathrm{d}}\frac{\partial^3 w}{\partial t\partial x^2} \\ = \rho A & \left[\frac{\partial^2 w}{\partial t^2} - (e_0a)^2\frac{\partial^4 w}{\partial t^2\partial x^2}\right]. \end{aligned} \tag{3.13}$$

To facilitate a good comparison between results, indirect parameters can be articulated as follows:

$$\begin{aligned} & X = \frac{x}{L},\ w_0 = \frac{W}{L},\ \gamma = \frac{e_0a}{L},\ K_{\mathrm{w}} = \frac{K_{\mathrm{w}}L^4}{\mathrm{EI}}, \\ & T_x = \frac{T_xL^2}{\mathrm{EI}}, N_x = \frac{N_xL^2}{\mathrm{EI}}, M_x = \frac{M_xL^2}{\mathrm{EI}},\ c_{\mathrm{d}} = c_{\mathrm{d}}\sqrt{\frac{L^4}{\mathrm{EI}}}\ , \\ & \Omega = \Omega\sqrt{\frac{\rho AL^4}{\mathrm{EI}}}. \end{aligned} \tag{3.14}$$

By incorporating these indirect parameters and substituting them into Eq. (3.9), the governing equation of nanobeam can be derived as follows:

$$\begin{aligned} \frac{\partial^4 w_0}{\partial X^4} - \Bigg\{ & M_x + T_x + N_x + F\cos\Omega t \\ & - \left[\frac{EA}{2L}\right]\int_0^L\left(\frac{\partial w_0}{\partial x}\right)^2 \mathrm{d}x\Bigg\}\frac{\partial^2 w_0}{\partial X^2} + c_d\frac{\partial w_0}{\partial t} + K_w w_0 \\ & + (\gamma)^2\frac{\partial^4 w_0}{\partial X^4}\Bigg\{M_x + T_x + N_x + Fcos\Omega t \\ & - \left[\frac{EA}{2L}\right]\int_0^L\left(\frac{\partial w_0}{\partial x}\right)^2 \mathrm{d}x\Bigg\} - (\gamma)^2K_{\mathrm{w}}\frac{\partial^2 w_0}{\partial X^2} \\ & - (\gamma)^2c_{\mathrm{d}}\frac{\partial^3 w_0}{\partial t\partial X^2} = \left(\frac{\partial^2 w_0}{\partial t^2} - (\gamma)^2\frac{\partial^4 w_0}{\partial t^2\partial X^2}\right) \end{aligned} \tag{3.15}$$

# 4 HPT

HPT offers an analytical approximate solution for problems that exhibit continuity within the solution domain. This technique involves considering a differential equation.

$$Ly + Ny = f(x),\ x\epsilon\Omega. \tag{4.1}$$

Under the boundary condition, $B\left(y, \frac{\partial y}{\partial x}\right) = 0, \quad x \in \Gamma$ . Here $L$ is the linear operator, $N$ is the nonlinear operator, $B$ is the boundary operator, Γ represents the boundary of the domain Ω, and $(x)$ is the known analytic function. HPT defines a homotopy as $\upsilon(x, p) = \Omega \times [0, 1] \to R$ that satisfies the following inequalities:

$$H(\upsilon, p) = (1 - p)[L(v) - L(y_0)] + p[L(v) + N(v) - f(x)] = 0, \tag{4.2}$$

or

$$H(\upsilon, p) = L(v) - L(y_0) + pL(y_0) + p[N(v) - f(x)] = 0, \tag{4.3}$$

where $x\epsilon\Omega$ and $p\epsilon\ [0, 1]$, and $y_0$ is an initial approximation that satisfies the boundary condition. Now from Eqs. (4.2) to (4.3) one can obtain

$$H(\upsilon, 0) = L(v) - L(y_0) = 0,$$

$$H(\upsilon, 1) = L(v) + N(v) - f(x) = 0. \tag{4.4}$$

In topology, $L(v) - L(y_0)$ and $L(v) + N(v) - f(x)$ are homotopic functions, indicating that there exists a continuous deformation between them through the homotopy parameter $p$.

Consider the power series solution of (4.2)–(4.3) as follows:

$$\upsilon = \upsilon_0 + p\upsilon_1 + p^2\upsilon_2 + p^3\upsilon_3 + .... \tag{4.5}$$

Hence, the approximate solution of (4.2) can be obtained

$$y = \lim_{p\to 1} v = v + \upsilon_0 + \upsilon_1 + \upsilon_2 + .... \tag{4.6}$$

## 4.1 Implementation of boundary conditions in HPT

Simply Supported–Simply Supported (S–S)

$$w_0 = \frac{\mathrm{d}^2 w_0}{\mathrm{d}x^2} = \frac{\mathrm{d}^4 w_0}{\mathrm{d}x^4} = 0 \text{ at } x = 0,$$

$$w_0 = \frac{\mathrm{d}^2 w_0}{\mathrm{d}x^2} = \frac{\mathrm{d}^4 w_0}{\mathrm{d}x^4} = 0 \text{ at } x = 1. \tag{4.7}$$

So after using the above boundary conditions in the $n$th order approximate solution the system of homogeneous equation can be written as

$$M(\lambda)[A\ B\ C\ D]^{\mathrm{T}} = 0. \tag{4.8}$$

For a nontrivial solution, determinant of coefficient matrix must be zero. The determinant of coefficient matrix yields a characteristic equation in terms of $\lambda$. Positive real roots of this equation are the normalized free vibration frequencies for the case considered.

## 4.2 HPT formulation for present problem

Consider the nondimensional differential Eq. (3.15), this equation can be reformulated as

$$\frac{\partial^4 w_0}{\partial X^4} = \frac{N}{\gamma^2 N - 1}\frac{\partial^2 w_0}{\partial X^2} + \frac{1}{\gamma^2 N - 1}\frac{\partial^2 w_0}{\partial t^2} - \frac{\gamma^2}{\gamma^2 N - 1}\frac{\partial^4 w_0}{\partial t^2 \partial X^2} - c_{\mathrm{d}}\frac{\partial w_0}{\partial t} - K_{\mathrm{w}} w_0. \tag{4.9}$$

The homotopy can be applied as [35]

$$\frac{\partial^4 w_0}{\partial X^4} = p\left[\frac{N}{\gamma^2 N - 1}\frac{\partial^2 w_0}{\partial X^2} + \frac{1}{\gamma^2 N - 1}\frac{\partial^2 w_0}{\partial t^2} - \frac{\gamma^2}{\gamma^2 N - 1}\frac{\partial^4 w_0}{\partial t^2 \partial X^2} - c_{\mathrm{d}}\frac{\partial w_0}{\partial t} - K_{\mathrm{w}} w_0\right], \tag{4.10}$$

where $p$ is the homotopy parameter, $p \in [0, 1]$. It is obvious that when $p = 0$, the equation becomes homogeneous, *i.e.*,

$$\frac{\partial^4 w}{\partial X^4} = 0. \tag{4.11}$$

The initial approximation $W_0$ is obtained by solving the homogeneous Eq. (4.11), hence

$$w_0 = Ax^4 + Bx^3 + Cx^2 + D. \tag{4.12}$$

The basic assumption of the HPT is that the solution of Eq. (4.10) can be written as a power series in $p$

$$w_{\mathrm{aprprox}} = w_0 + pw_1 + p^2 w_2 + .... \tag{4.13}$$

By substituting the value of $w_{\mathrm{aprprox}}$ from Eq. (4.13) in Eq. (4.10)

$$\begin{aligned}\frac{\partial^4}{\partial X^4}[w_0 + pw_1 + p^2 w_2 + ...] &= p\left[\frac{N}{\gamma^2 N - 1}\frac{\partial^2}{\partial X^2}[w_0 + pw_1 + p^2 w_2 + ...]\right. \\ &+ \frac{1}{\gamma^2 N - 1}\frac{\partial^2}{\partial t^2}[w_0 + pw_1 + p^2 w_2 + ...] \\ &- \frac{\gamma^2}{\gamma^2 N - 1}\frac{\partial^4}{\partial t^2 \partial X^2}\left[w_0 + pw_1 + p^2 w_2\right. \\ &\left.\left. + ...\right] - c_{\mathrm{d}}\frac{\partial}{\partial t}\left[w_0 + pw_1 + p^2 w_2 + ...\right] - k_{\mathrm{w}}[w_0 \right. \\ &\left.\left. + pw_1 + p^2 w_2 + ...\right]\right].\end{aligned} \tag{4.14}$$

Now comparing the coefficients of $p$ in Eq. (4.14), the recurrence relation can be obtained as

$$\frac{\partial^4 w_i}{\partial X^4} = \left[\frac{N}{\gamma^2 N - 1}\frac{\partial^2 w_{i-1}}{\partial X^2} + \frac{1}{\gamma^2 N - 1}\frac{\partial^2 w_{i-1}}{\partial t^2} - \frac{\gamma^2}{\gamma^2 N - 1}\frac{\partial^4 w_{i-1}}{\partial t^2 \partial X^2} - c_{\mathrm{d}}\frac{\partial w_{i-1}}{\partial t} - K_{\mathrm{w}} w_{i-1}\right], \tag{4.15}$$

where $i \geq 1$ and initial guess $w_0$ is given in Eq. (4.12). The solution to Eq. (4.9) can be approximated as per the study of He [24].

$$w_0 = \lim_{p \to 1} w_{\mathrm{aprrox}} = w_0 + w_1 + w_2 + .... \tag{4.16}$$

The convergence of the series in Eq. (4.16) is proved in previous studies [24,30].

## 5 Numerical results

In this section, numerical results are examined based on the application of both thermo-magneto-mechanical loading and external parametric excitation. The focus lies in understanding the impact of parametric excitation through the examination of instability regions and bifurcation points. To aid comprehension, key parameters are defined across various regions of the graph. This helps to elucidate the concepts and enhance clarity. The system's material properties, including those of the nanobeam and elastic matrix, consist of the following parameters: Temperature $T$ = 300 K, Poisson's ratio of the beam material $\nu$ = 0.3, Winkler coefficient $k_{\mathrm{w}}$ = 0.5 GPa, and a viscoelastic damping coefficient $c_{\mathrm{d}} = 3 \times 10^{-7}$ Pa s. Additionally, the nanobeam diameter $d$ = 3 nm and the small-scale parameter are considered to be smaller than 2 nm according to the study of Reddy [32]. One can explore its dependence on several factors, including the scaling parameter, porosity pattern, and nonlocal effects. To do this, a set of material constants are taken in Table 1.

First, to verify the accuracy of the formulation, Table 2 is presented. The numerical results of the present study reported in the table are compared with other available research studies and literature [20,50] so that, they are partly similar and close to our research. Table 2 shows the nonlinear frequency ratio ($\omega_{\mathrm{NL}}, \omega_{\mathrm{L}}$) for amplitude-to-radius ($\omega_{\max}/r$) ratio of isotropic beam with simply supported boundary conditions. The nonlinear frequency ratio is tabled for different amplitude ratios [1–3]. The results presented in the study of Nazemnezhad and Hosseini-Hashemi [20] are consistent with the numerical results of the present work as a similar analytical approach was used in both.

**Table 1:** Beam dimensions and their material properties [26]

| Parameter | Value (unit) | Description |
|---|---|---|
| $a$ | 0.5 m | Length of the beam |
| $b$ | 0.05 m | Width of the beam |
| $h$ | 0.05 m | Height of the beam |
| $E$ | 1,100 GPa | Young's modulus |
| $\rho$ | 1.3 g/cm$^3$ | Mass density |

**Table 2:** Frequency ratio ($\omega_{\mathrm{NL}}, \omega_{\mathrm{L}}$) at different maximum amplitude-to-radius ($\omega_{\max}/r$) ratios of isotropic beam with simply supported boundary conditions

| Amplitude ratio | Ref. [20] | Ref. [50] | Present work |
|---|---|---|---|
| 1 | 1.0937 | 1.0892 | 1.0758 |
| 2 | 1.3750 | 1.3178 | 1.3690 |
| 3 | 1.8438 | 1.6257 | 1.8401 |

Figure 2 illustrates that the relationship between the nonlinear frequency and the amplitude of the parametric excitation varies depending on the nondimensional damping coefficient $c_{\mathrm{d}}$. When $c_{\mathrm{d}}$ is low, indicating less damping in the system, higher oscillation amplitudes are achievable. Consequently, the nonlinear frequency tends to be higher in such cases. This implies that the nonlinear frequency increases together with a rise in the parametric excitation amplitude, producing a more intense nonlinear response. In summary, lower values of $c_{\mathrm{d}}$ cause the nonlinear frequency to decrease as the amplitude increases, whereas lower values of the nondimensional damping coefficient cause the nonlinear frequency to increase with increasing amplitude of parametric stimulation. Figure 3 displays the relationship between the force amplitude and the nonlinear frequency amplitude concerning the nondimensional Winkler coefficient $k_{\mathrm{w}}$. The

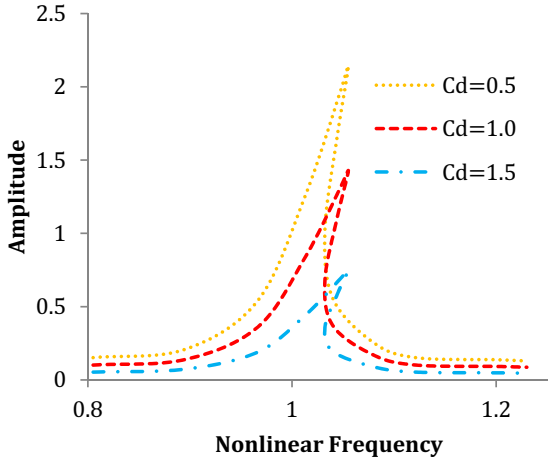


**Figure 2:** The effect of nonlinear frequency on the amplitude of parametric excitation for different values of damping coefficient ($c_{\mathrm{d}}$).

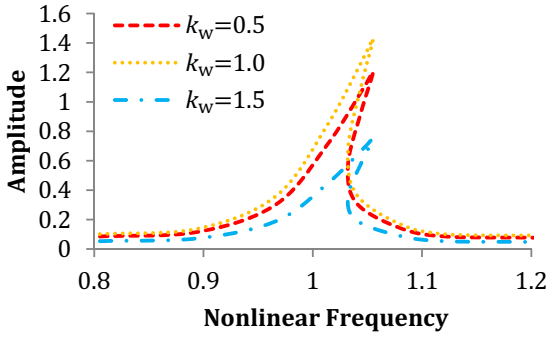


**Figure 3:** The effect of nonlinear frequency on the amplitude of parametric excitation for different values of Winkler coefficient ($k_w$).

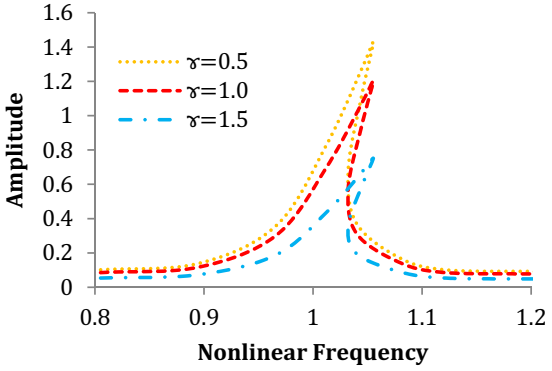


**Figure 5:** The effect of nonlinear frequency on the amplitude of parametric excitation for different values of nonlocal parameter ($\gamma$).

graph illustrates that as the Winkler coefficient increases and the force amplitude decreases. However, it is noteworthy that the Winkler coefficient does not influence the occurrence of bifurcation points. In other words, while changes in $k_w$ affect the force amplitude; they do not impact the system's bifurcation behavior. Figure 4 shows how, for a range of uniaxial magnetic field values, the nonlinear frequency varies with the magnitude of parametric excitation. The force nonlinear frequency of a system subjected to a uniaxial magnetic field denotes the frequency at which the system's response turns nonlinear as a result of the magnetic field's effect. The system's response to the magnetic field may exhibit nonlinear behavior as the amplitude of parametric stimulation increases, resulting in changes in the nonlinear frequency. Figure 5 illustrates the nonlocal parameter's effect on the nonlinear frequency–response curves. It is clear from the graph that increasing the nonlocal parameter reduces the hardening behavior while enhancing the bending stiffness. The relationship between the parametric excitation amplitude and the force amplitude of the nonlinear frequency is shown for different temperatures in Figure 6. Additionally, it is observed that an increase in the temperature gradient results in a higher amplitude at the lower limit point bifurcation. Conversely, elevating the initial imperfection amplitude leads to greater response amplitude at the higher limit point bifurcation. Figure 7 illustrates the impact of varying the parameter excitation on the amplitude concerning the Winkler coefficient $k_w$. Notably, as the parameter excitation declines in the amplitude of the Winkler coefficient and damps at some point (0.1–0.15). Nevertheless, amplitude 1 shows a growing trend while the parametric excitation keeps increasing. Moreover, it is worth noting that the smallest amplitudes occur at a parametric excitation level of $k_w$ = 1.5. In Figure 8, the amplitude for a system under parametric excitation depends on both the force amplitude $k$ and the nondimensional damping coefficient $c_d$. Lower damping generally leads to larger amplitudes near resonance, while higher damping suppresses oscillations and keeps the amplitude relatively low. Critical damping minimizes the amplitude of the system's response.

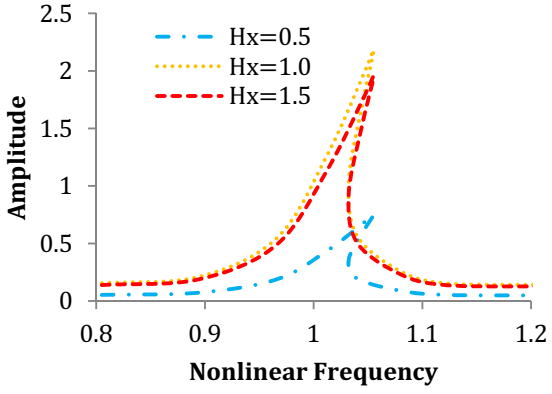


**Figure 4:** The effect of nonlinear frequency on the amplitude of parametric excitation for different values of uniaxial magnetic field ($H_x$).

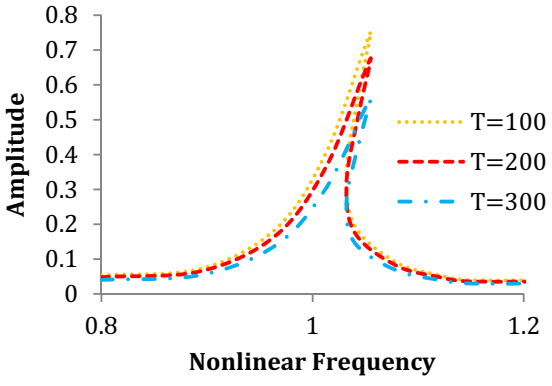


**Figure 6:** The effect of nonlinear frequency on the amplitude of parametric excitation for different values of temperature ($T$).

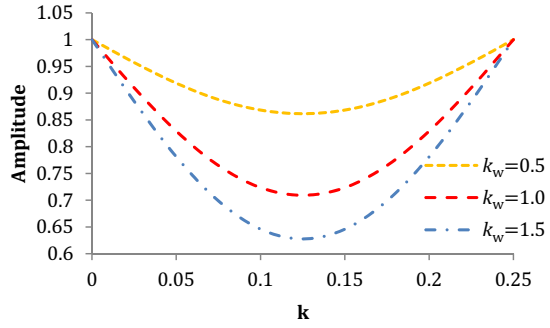


**Figure 7:** The effect of parametric excitation on the amplitude of parametric excitation for different values of Winkler coefficient ($k_w$).

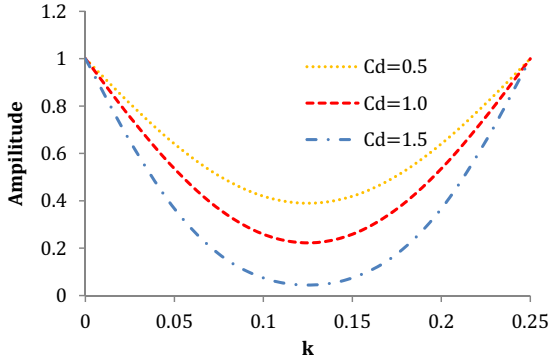


**Figure 8:** The effect of parametric excitation on the amplitude of parametric excitation for different values of damping coefficient ($c_d$).

In Figure 9, the effect of changing the parametric excitation on the amplitude is demonstrated concerning the uniaxial magnetic field $H_x$. Initially, the parameter excitation declines in the amplitude and damps at some point (0.1–0.15). However, as the parametric excitation continues to increase, the amplitude exhibits a rising trend.

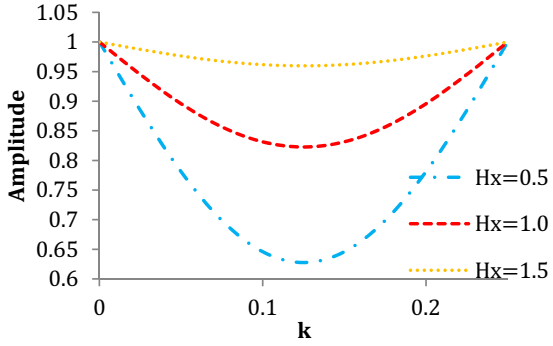


**Figure 9:** The effect of parametric excitation on the amplitude of parametric excitation for different values of uniaxial magnetic field ($H_x$).

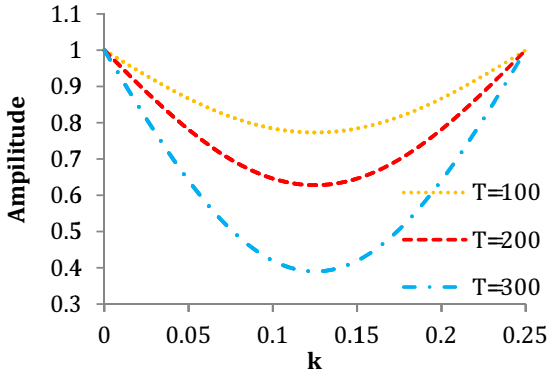


**Figure 10:** The effect of parametric excitation on the amplitude of parametric excitation for different values of temperature ($T$).

Additionally, it is noteworthy that the smallest amplitudes are observed at a parametric excitation level of $H_x$ = 0.5. The relationship between the parametric excitation and amplitude for various temperature levels is depicted in Figure 10. It is found that a gradual decrease in temperature starting around 1.0 and damping at some point (0.1–0.15). On the other hand, the amplitude shows a rising trend while the parametric excitation keeps increasing. Additionally, it is noteworthy that the smallest amplitudes are observed at a parametric excitation level of $T$ = 300. In Figure 11, the relationship between parametric excitation and amplitude is illustrated across various values of the nondimensional nonlocal parameter $\gamma$. As the $\gamma$ value gradually decreases, starting from approximately 1.0 and tapering off between 0.1 and 0.15, a resonant behavior is evident. This resonance is attributed to the combined effects of parametric excitation and amplitude on the system. Figures 12 and 13 show the stress contours of the magneto-thermo-elastic nanobeam for different porosity distributions. We can find that the stress change zone is restricted in a finite area and the stress does

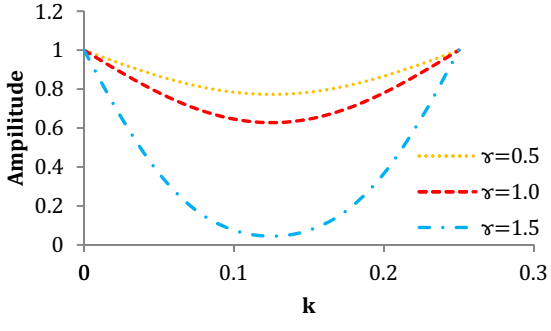


**Figure 11:** The effect of parametric excitation on the amplitude of parametric excitation for different values of nondimensional nonlocal parameter ($\gamma$).

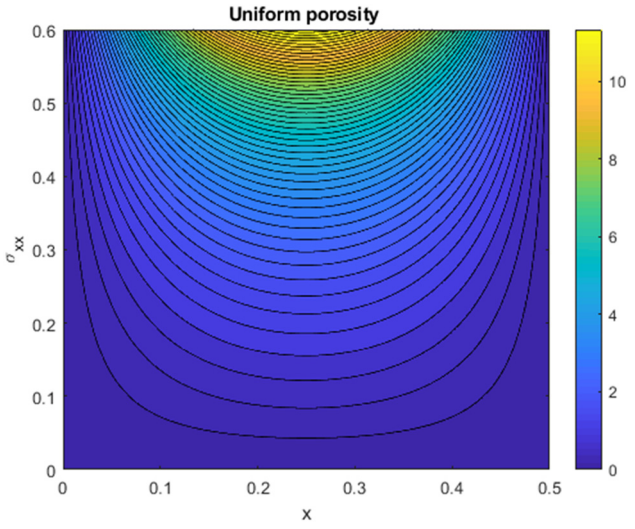


**Figure 12:** The contour plot of the stress distribution for uniform porosity with $e_0 = 0$.

not change out of this area. The blue color in these figures refers to a stress variation of zero in this region. We can observe that the region with changes in stress becomes larger with lower nonlocal values.

## 6 Conclusions

The aim of this research is to examine the dynamic parametric excitation and nonlinear vibration behavior of Euler–Bernoulli porous nanobeams under thermo-magneto-mechanical loading. Initially, a concise model of the Euler–Bernoulli nanobeam is developed and subjected to parametric external excitation. Utilizing the nonlocal continuum theory and nonlinear von Karman beam theory, the governing nonlinear differential equation of motion is derived. The partial differential equation is then converted into an ordinary differential equation using the HPT. Next, the Euler–Bernoulli nanobeam modulation equation is found. Special attention is given to the influence of parametric excitation, and bifurcation points are scrutinized to delineate instability regions. Notably, it is observed that the damping coefficient, along with parametric excitation, significantly affects the system stability and frequency responsiveness. Thermo-magneto-mechanical loads are found to induce either growth or decay in the amplitude. The following is a list of the study's other main results:

- The influence of parametric excitation induced by an external axial force on system stability is substantial.
- The damping coefficient significantly influences system stability, while factors such as the nonlocal parameter and Winkler coefficient are of less importance.
- Amplitude response is observed to vary as a function of the excitation frequency. For initial amplitudes of significant magnitude, the response decays until reaching a steady-state solution.
- An increase in force amplitude leads to a notable separation between stable and unstable curves, creating a gap between them.
- Nano-size beam having nonuniform pores 2 results in greater vibration frequency.
- Results demonstrate that physical variables significantly influence both nonlinear frequency behavior and parametric excitation. The numerical results serve as reference points for conducting further analyses of nanobeams, which serve as fundamental components in nano-electromechanical systems.

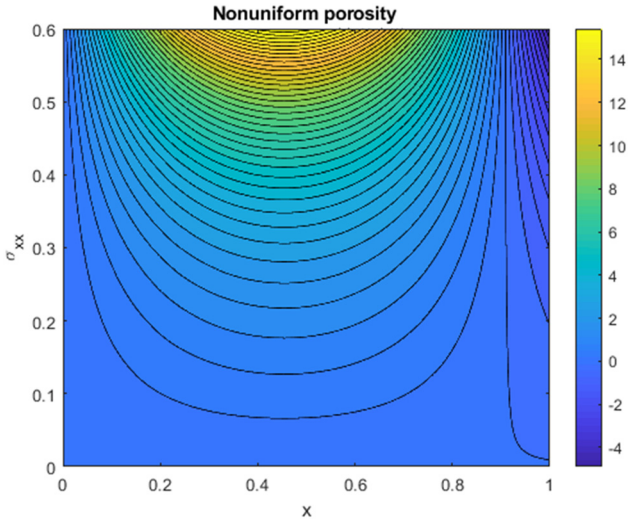


**Figure 13:** The contour plot of the stress distribution for Nonuniform porosity with $e_0 = 0.5$.

**Funding information:** The authors state no funding involved.

**Author contributions:** All authors have accepted responsibility for the entire content of this manuscript and consented to its submission to the journal, reviewed all the results, and approved the final version of the manuscript. RS and LA conceived of the presented idea, developed the theory, and performed the computations. LV verified the analytical methods. RD and FT supervised the finding of this entire work. All authors discussed the results and contributed to the final manuscript.

**Conflict of interest:** Authors F.T. and R.D., who are the co-authors of this article, are current Editorial Board

members of Curved and Layered Structures. This fact did not affect the peer-review process, and it was handled entirely by other editors of the journal. The authors declare no other conflict of interest.

## References


[1] Eda G, Fanchini G, Chhowalla M. Large-area ultrathin films of reduced graphene oxide as a transparent and flexible electronic material. Nat Nanotechnol. 2008;3(5):270–4. doi: 10.1038/nnano.2008.83.

[2] Li D, Müller MB, Gilje S, Kaner RB, Wallace GG. Processable aqueous dispersions of graphene nanosheets. Nat Nanotechnol. 2008;3(2):101–5. doi: 10.1038/nnano.2007.451.

[3] Potekin R, Kim S, McFarland DM, Bergman LA, Cho H, Vakakis AF. A micromechanical mass sensing method based on amplitude tracking within an ultra-wide broadband resonance. Nonlinear Dyn. 2018;92:287–304. doi: 10.1007/s11071-018-4055-y.

[4] Mahmoud MA. Validity and accuracy of resonance shift prediction formulas for microcantilevers: a review and comparative study. Crit Rev Solid State Mater Sci. 2016;41(5):386–429. doi: 10.1080/10408436.2016.1142858.

[5] Ji Y, Choe M, Cho B, Song S, Yoon J, Ko HC, et al. Organic nonvolatile memory devices with charge trapping multilayer graphene film. Nanotechnology. 2012;23(10):105202. doi: 10.1088/0957-4484/23/10/105202.

[6] Arash B, Wang Q. Detection of gas atoms with carbon nanotubes. Sci Rep. 2013;3(1):1782. doi: 10.1038/srep01782.

[7] Bunch JS, Van Der Zande AM, Verbridge SS, Frank IW, Tanenbaum DM, Parpia JM, et al. Electromechanical resonators from graphene sheets. Science. 2007;315(5811):490–3. doi: 10.1126/science.1136836.

[8] Kuilla T, Bhadra S, Yao D, Kim NH, Bose S, Lee JH. Recent advances in graphene based polymer composites. Prog Polym Sci. 2010;35(11):1350–75. doi: 10.1016/j.progpolymsci.2010.07.005.

[9] Eringen AC, Edelen D. On nonlocal elasticity. Int J Eng Sci. 1972;10(3):233–48.

[10] Eringen AC. Theories of nonlocal plasticity. Int J Eng Sci. 1983;21(7):741–51. doi: 10.1016/0020-7225(83)90058-7.

[11] Ghadiri M, Shafiei N, Akbarshahi A. Influence of thermal and surface effects on vibration behavior of nonlocal rotating Timoshenko nanobeam. Appl Phys A. 2016;122:1–9. doi: 10.1007/s00339-016-0196-3.

[12] Sudak LJ. Column buckling of multiwalled carbon nanotubes using nonlocal continuum mechanics. J Appl Phys. 2003;94(11):7281–7. doi: 10.1063/1.1625437.

[13] Zhang YQ, Liu GR, Wang JS. Small-scale effects on buckling of multiwalled carbon nanotubes under axial compression. Phys Rev B. 2004;70(20):205430. doi: 10.1103/PhysRevB.70.205430.

[14] Barretta R, Feo L, Luciano R, de Sciarra FM. Variational formulations for functionally graded nonlocal Bernoulli–Euler nanobeams. Compos Struct. 2015;129:80–9. doi: 10.1016/j.compstruct.2015.03.033.

[15] Ghadiri M, Safi M. Nonlinear vibration analysis of functionally graded nanobeam using homotopy perturbation method. Adv Appl Math Mech. 2017;9(1):144–56. doi: 10.4208/aamm.2015.m899.

[16] Ehyaei J, Akbarshahi A, Shafiei N. Influence of porosity and axial preload on vibration behavior of rotating FG nanobeam. Adv Nano Res. 2017;5(2):141. doi: 10.12989/anr.2017.5.2.141.

[17] Ebrahimi F, Hosseini SH. Thermal effects on nonlinear vibration behavior of viscoelastic nanosize plates. J Therm Stresses. 2016;39(5):606–25. doi: 10.1080/01495739.2016.1160684.

[18] Şimşek M. Large amplitude free vibration of nanobeams with various boundary conditions based on the nonlocal elasticity theory. Compos Part B: Eng. 2014;56:621–8. doi: 10.1016/j.compositesb.2013.08.082.

[19] Şimşek M. Nonlinear free vibration of a functionally graded nanobeam using nonlocal strain gradient theory and a novel Hamiltonian approach. Int J Eng Sci. 2016;105:12–27. doi: 10.1016/j.ijengsci.2016.04.013.

[20] Nazemnezhad R, Hosseini-Hashemi S. Nonlocal nonlinear free vibration of functionally graded nanobeams. Compos Struct. 2014;110:192–9. doi: 10.1016/j.compstruct.2013.12.006.

[21] Nourbakhsh H, Mohammadzadeh R, Rafiee M, Rafiee R. Nonlinear effects on resonance behaviour of beams in micro scale. Appl Mech Mater. 2012;110:4178–86. doi: 10.4028/www.scientific.net/AMM.110-116.4178.

[22] Oskouie MF, Ansari R, Sadeghi F. Nonlinear vibration analysis of fractional viscoelastic Euler–Bernoulli nanobeams based on the surface stress theory. Acta Mech Solida Sin. 2017;30(4):416–24. doi: 10.1016/j.camss.2017.07.003.

[23] Ghadiri M, Rajabpour A, Akbarshahi A. Non-linear forced vibration analysis of nanobeams subjected to moving concentrated load resting on a viscoelastic foundation considering thermal and surface effects. Appl Math Model. 2017;50:676–94. doi: 10.1016/j.apm.2017.06.019.

[24] He JH. A coupling method of a homotopy technique and a perturbation technique for non-linear problems. Int J Non-Linear Mech. 2000;35(1):37–43. doi: 10.1016/S0020-7462(98)00085-7.

[25] Barati MR. Nonlocal-strain gradient forced vibration analysis of metal foam nanoplates with uniform and graded porosities. Adv Nano Res. 2017;5(4):393. doi: 10.12989/anr.2017.5.4.393.

[26] Kováčik J, Marsavina L, Linul E. Poisson's ratio of closed-cell aluminium foams. Materials. 2018;11(10):1904. doi: 10.3390/ma11101904.

[27] Pourjabari A, Hajilak ZE, Mohammadi A, Habibi M, Safarpour H. Effect of porosity on free and forced vibration characteristics of the GPL reinforcement composite nanostructures. Comput Math Appl. 2019;77(10):2608–26. doi: 10.1016/j.camwa.2018.12.041.

[28] Chen D, Yang J, Kitipornchai S. Free and forced vibrations of shear deformable functionally graded porous beams. Int J Mech Sci. 2016;108:14–22. doi: 10.1016/j.ijmecsci.2016.01.025.

[29] Mirjavadi SS, Afshari BM, Barati MR, Hamouda AM. Nonlinear free and forced vibrations of graphene nanoplatelet reinforced microbeams with geometrical imperfection. Microsyst Technol. 2019;25:3137–50. doi: 10.1007/s00542-018-4277-4.

[30] He JH. Addendum: new interpretation of homotopy perturbation method. Int J Mod Phys B. 2006;20(18):2561–8. doi: 10.1142/S0217979206034819.

[31] Eltaher MA, Mahmoud FF, Assie AE, Meletis E. Coupling effects of nonlocal and surface energy on vibration analysis of nanobeams. Appl Math Comput. 2013;224:760–74. doi: 10.1016/j.amc.2013.09.002.

[32] Reddy J. Nonlocal theories for bending, buckling and vibration of beams. Int J Eng Sci. 2007;45(2–8):288–307. doi: 10.1016/j.ijengsci.2007.04.004.

[33] Aydogdu M. A general nonlocal beam theory: its application to nanobeam bending, buckling and vibration. Phys E: Low-Dimension Syst Nanostruct. 2009;41(9):1651–5. doi: 10.1016/j.physe.2009.05.014.
[34] Alevras P, Theodossiades S, Rahnejat H. Broadband energy harvesting from parametric vibrations of a class of nonlinear Mathieu systems. Appl Phys Lett. 2017;110(23):233901. doi: 10.1063/1.4984059.
[35] Amer YA, El-Sayed AT, Kotb AA. Nonlinear vibration and of the Duffing oscillator to parametric excitation with time delay feedback. Nonlinear Dyn. 2016;85:2497–505. doi: 10.1007/s11071-016-2840-z.
[36] Bobryk RV, Yurchenko D. On enhancement of vibration-based energy harvesting by a random parametric excitation. J Sound Vib. 2016;366:407–17. doi: 10.1016/j.jsv.2015.11.033.
[37] Darabi M, Ganesan R. Non-linear vibration and dynamic instability of internally-thickness-tapered composite plates under parametric excitation. Compos Struct. 2017;176:82–104. doi: 10.1016/j.compstruct.2017.04.059.
[38] Wang YZ. Nonlinear internal resonance of double-walled nanobeams under parametric excitation by nonlocal continuum theory. Appl Math Model. 2017;48:621–34. doi: 10.1016/j.apm.2017.04.018.
[39] Krylov S, Harari I, Cohen Y. Stabilization of electrostatically actuated microstructures using parametric excitation. J Micromech Microeng. 2005;15(6):1188. doi: 10.1088/0960-1317/15/6/009.
[40] Yan Q, Ding H, Chen L. Nonlinear dynamics of axially moving viscoelastic Timoshenko beam under parametric and external excitations. Appl Math Mech. 2015;36(8):971–84. doi: 10.1007/s10483-015-1966-7.
[41] Eringen AC. Nonlocal polar elastic continua. Int J Eng Sci. 1972;10(1):1–6. doi: 10.1016/0020-7225(72)90070-5.
[42] Eringen AC. On differential equations of nonlocal elasticity and solutions of screw dislocation and surface waves. J Appl Phys. 1983;54(9):4703–10. doi: 10.1063/1.332803.
[43] Reddy JN. An introduction to continuum mechanics. United Kingdom: Cambridge University Press; 2013.
[44] Reddy J. Nonlocal nonlinear formulations for bending of classical and shear deformation theories of beams and plates. Int J Eng Sci. 2010;48(11):1507–18. doi: 10.1016/j.ijengsci.2010.09.020.
[45] Emam SA. A static and dynamic analysis of the postbuckling of geometrically imperfect composite beams. Compos Struct. 2009;90(2):247–53. doi: 10.1016/j.compstruct.2009.03.020.
[46] Emam SA, Nayfeh AH. Postbuckling and free vibrations of composite beams. Compos Struct. 2009;88(4):636–42. doi: 10.1016/j.compstruct.2008.06.006.
[47] Murmu T, McCarthy MA, Adhikari S. In-plane magnetic field affected transverse vibration of embedded single-layer graphene sheets using equivalent nonlocal elasticity approach. Compos Struct. 2013;96:57–63. doi: 10.1016/j.compstruct.2012.09.005.
[48] Kitipornchai S, He XQ, Liew KM. Continuum model for the vibration of multilayered graphene sheets. Phys Rev B. 2005;72(7):075443. doi: 10.1103/PhysRevB.72.075443.
[49] Nayfeh AH, Mook DT. Nonlinear oscillations. USA: John Wiley & Sons; 2008.
[50] Azrar L, Benamar R, White RG. Semi-analytical approach to the non-linear dynamic response problem of S–S and C–C beams at large vibration amplitudes part I: general theory and application to the single mode approach to free and forced vibration analysis. J Sound Vib. 1999;224(2):183–207. doi: 10.1006/jsvi.1998.1893.
[51] Azrar L, Benamar R, White RG. A semi-analytical approach to the non-linear dynamic response problem of beams at large vibration amplitudes, part ii: multimode approach to the steady state forced periodic response. J Sound Vib. 2002;255(1):141. doi: 10.1006/jsvi.2000.3595.
[52] Ebrahimi F, Kokaba M, Shaghaghi G, Selvamani R. Dynamic characteristics of hygro-magneto-thermo-electrical nanobeam with non-ideal boundary conditions. Adv Nano Res. 2020;8(2):169–82. doi: 10.12989/anr.2020.8.2.169.
[53] Selvamani R, Loganathan R, Dimitri R, Tornabene F. Nonlocal state-space strain gradient wave propagation of magneto thermo piezoelectric functionally graded nanobeam. Curved Layer Struct. 2023;10(1):20220192. doi: 10.1515/cls-2022-0192.
[54] Selvamani R, Rexy J, Ebrahimi F. Two phase local/non local waves in a magneto thermo electrical composite nano beam reinforced with graphene oxide powder. Waves Random Complex Media. 2021;34(5):1–26. doi: 10.1080/17455030.2021.1985745.
[55] Anitha L, Rajalakshmi L, Selvamani R, Ebrahimi F. Forced nonlinear vibrations in a smart magneto-viscoelastic multiscale composite nanobeam in a humid thermal environment. Eng Trans. 2023;71(4):617–44. doi: 10.24423/EngTrans.3114.20231121.
[56] Selvamani R, Rexy J, Ebrahami F. Vibration in an electrically affected hygro-magneto-thermo-flexo electric nanobeam embedded in winkler-pasternak foundation. Mech Adv Compos Struct. 2021;8(2):401–14. doi: 10.22075/macs.2021.22068.1311.
[57] Selvamani R, Rubine L, Rexy J, Ebrahimi F. Dispersion analysis of electrically actuated hygro-magneto-thermo-flexo electric nanobeam embedded on silica aerogel foundation. Mater Phys Mech. 2022;50(1):1–19. doi: 10.18149/MPM.5012022_1.